Article No. jmbi.1999.3179 available online at http://www.idealibrary.com on IDEAL® J. Mol. Biol. (1999) 293, 595–611

JMB

X-ray Structure Determination of a Vanadium-dependent Haloperoxidase from *Ascophyllum nodosum* at 2.0 Å Resolution

M. Weyand[1]*, H.-J. Hecht[1], M. Kieß[1], M.-F. Liaud[2], H. Vilter[1] and D. Schomburg[1]

[1]*GBF (Gesellschaft für Biotechnologische Forschung) Department of Molecular Structure Research Mascheroder Weg 1 D-38124, Braunschweig Germany*

[2]*Technical University Carolo Wilhelmina at Braunschweig Institute of Genetics Spielmannstraße 7 D-38106, Braunschweig Germany*

**Corresponding author*

The homo-dimeric structure of a vanadium-dependent haloperoxidase (V-BPO) from the brown alga *Ascophyllum nodosum* (EC 1.1.11.X) has been solved by single isomorphous replacement anomalous scattering (SIRAS) X-ray crystallography at 2.0 Å resolution (PDB accession code 1QI9), using two heavy-atom datasets of a tungstate derivative measured at two different wavelengths. The protein sequence (SwissProt entry code P81701) of V-BPO was established by combining results from protein and DNA sequencing, and electron density interpretation. The enzyme has nearly an all-helical structure, with two four-helix bundles and only three small β-sheets. The holoenzyme contains trigonal-bipyramidal coordinated vanadium atoms at its two active centres. Structural similarity to the only other structurally characterized vanadium-dependent chloroperoxidase (V-CPO) from *Curvularia inaequalis* exists in the vicinity of the active site and to a lesser extent in the central four-helix bundle.

Despite the low sequence and structural similarity between V-BPO and V-CPO, the vanadium binding centres are highly conserved on the N-terminal side of an α-helix and include the proposed catalytic histidine residue ($His418^{V\text{-}BPO}$/$His404^{V\text{-}CPO}$). The V-BPO structure contains, in addition, a second histidine near the active site ($His411^{V\text{-}BPO}$), which can alter the redox potential of the catalytically active VO_2-O_2 species by protonation/deprotonation reactions. Specific binding sites for the organic substrates, like indoles and monochlordimedone, or for halide ions are not visible in the V-BPO structure. A reaction mechanism for the enzymatic oxidation of halides is discussed, based on the present structural, spectroscopic and biochemical knowledge of vanadium-dependent haloperoxidases, explaining the observed enzymatic differences between both enzymes.

Keywords: vanadium; bromoperoxidase; chloroperoxidase; X-ray structure; sequence determination

Present addresses: H. Vilter, Zurmaiener Straße 16, D-54292 Trier, Germany; D. Schomburg, University of Cologne, Institute of Biochemistry, Zuelpicher Straße 47, D-50674 Cologne, Germany; M. Weyand, Max-Planck-Institute for Molecular Physiology Otto-Hahn-Straße 11, D-44227 Dortmund, Germany.

Abbreviations used: V-BPO, vanadium-dependent haloperoxidase from *Ascophyllum nodosum*; V-HPO, vanadium-dependent haloperoxidases; V-CPO, vanadium-dependent chloroperoxidase from *Curvularia inaequalis*; V-CPO-N_3, V-CPO structure in azide form; V-CPO-VO_4, V-CPO holoenzyme structure; V-CPO-O_2, V-CPO structure in VO_2-peroxo form; SIRAS, single isomorphous replacement with anomalous scattering; PDB, Protein Data Bank; PVP, polyvinylpyrollidone; TFA, trifluoroacetic acid; PTH, phenylthiohydankoin; NCS, non-crystallographic symmetry.

E-mail address of the corresponding author:
michael-weyand@mpi-dortmund.mpg.de

0022-2836/99/430595–17 $30.00/0

Introduction

Haloperoxidases catalyse the oxidation of halides in the presence of peroxides and are referred as iodo-, bromo- or chloroperoxidase according to their ability to oxidize iodide, bromide or chloride. As a subgroup of peroxidases with broader specificity, like horseradish peroxidase, they are grouped according to their prosthetic co-factor into heme-containing and non-heme-containing enzymes, which are further subdivided in metal-free and vanadium-dependent haloperoxidases. Haloperoxidases are of broad interest in industrial catalysis for their ability to catalyse the halogenation of organic compounds. The use of heme-containing enzymes in this application has the disadvantage of low substrate specificity and unsatisfactory stability due to rapid oxidation and cleavage of the prosthetic heme ligand. The detection of non-heme-containing peroxidases, especially those containing vanadium (V) (Vilter, 1995), therefore seemed very promising for technical applications. Vanadium-dependent peroxidases, first detected in the brown alga *Ascophyllum nodosum* (Vilter, 1984) are very common in brown algae, but are known also from red algae, fungi and lichen.

The vanadium-dependent haloperoxidases exclusively catalyse the oxidation of halides, organic substrates are halogenated or oxidized subsequently due to the formation of hypo-halides. For technical applications, the high stability of these enzymes, their substrate specificity and availability from large-scale processes (Vilter, 1994) or expression systems (Simons *et al.*, 1995) is of interest. With respect to the structure and reaction mechanism of the vanadium-dependent haloperoxidases, intensive studies using several spectroscopic methods (for references, see Vilter, 1995) yielded only limited information. Therefore, three different vanadium-dependent peroxidases have been crystallized (Müller-Fahrnow *et al.*, 1988; Rush *et al.*, 1995; Weyand *et al.*, 1996; Messerschmidt & Wever, 1996; Brindley *et al.*, 1998) and the first structure of a vanadium-dependent haloperoxidase, the chloroperoxidase from *Curvularia inaequalis*, solved by Messerschmidt & Wever (1996), provided structural insights into the enzymatic oxidation of halides. The X-ray structure determination of the vanadium-dependent bromoperoxidase V-BPO from *Ascophyllum nodosum*, described here, allows the discussion of the observed differences in substrate specificity based on a comparison of both HPO sequences and structures, and based on a common reaction mechanism for vanadium-dependent haloperoxidases.

Results and Discussion

Establishment of the complete sequence

The brown alga *A. nodosum* contains more than one isoenzyme of V-BPO (Vilter 1983b; Krenn *et al.*, 1989; Vilter, 1995). Isolation of high-quality RNA from *A. nodosum* proved to be difficult due to the high content of alginates, fucan sulphates and tannins. Therefore, it was not possible to obtain full-length DNA clones (Vilter, 1995). DNA sequencing yielded partial sequences of several isoenzymes that were compared to peptide sequences. Due to the N-terminal blocked sequence and the lack of a corresponding DNA clone, the sequence for the N-terminal first 14 residues was established from the X-ray density. The molecular mass calculated on the basis of this sequence is 120,513 Da for the V-BPO homo-dimer, which is in the error range of the reported molecular mass established by mass spectroscopy of 120,413(±200) Da (Vilter, 1995). The present protein sequence is shown in Figure 1.

Quality of the structure model

The final V-BPO-model at the resolution of 2.0 Å consists of 1111 amino acid residues, two vanadate groups and 1787 water molecules. Three solvent-accessible tyrosine residues (TyrA398, TyrA447 and TyrB447) showed residual electron density in the *ortho*-position to the hydroxyl group. It is known that several enzymes of the brown alga *A. nodosum* are iodinated (Küpper *et al.*, 1998). Therefore, this electron density was interpreted as mono-iodinated tyrosine. In both monomers, Tyr447 shows residual electron density on both sides of the side-chain hydroxyl group (Figure 2). As the sites are not fully occupied, it is not possible to discriminate between a di-iodinated tyrosine residue and two side-chain conformations of a mono-iodinated tyrosine residue. During the refinement, the occupancies for both iodine atoms were manually varied until a SigmaA weighted $mF_o - DF_c$ map showed no residual density. In the final model, both atoms have an occupancy of 0.5, which may indicate mono-iodinated tyrosine residues in two different conformations. The occupancy for the iodine atom in TyrA398 was manually established as only 0.1. TyrB398, which is buried by a symmetry-related molecule, shows no residual electron density. This lack of iodination of TyrB398 may indicate that iodination of the tyrosine residues occurred after crystallization by soaking of the protein crystals with iodine and hydrogen peroxide.

The overall model has a crystallographic *R*-factor of 16.5 % (R_{free} 21.9 %) and shows continuous electron density for all atoms with the exception of some solvent-accessible side-chain atoms on the protein surface and for the pyro-glutamate (see Materials and Methods) at the N terminus of monomer A, which is not included in the final model. The RMS deviation for C^{α} atoms of both monomers is $RMS_{C\alpha} = 0.233$ and for all protein atoms $RMS_{all} = 0.475$. The average temperature factors are $B_{aveA} = 7.1$ Å^2 and $B_{aveB} = 7.0$ Å^2 for protein atoms of monomer B and A, respectively. The vanadate groups have average temperature factors of $B_{aveVO4A} = 2.9$ Å^2, $B_{aveVO4B} = 4.1$ Å^2 and

```
1    QTCSTSDDAD DPTPPNERDD EAFASRVAAA KRELEGTGTV CQINNGETDL   50
     ========== ====
51   AAKFHKSLPH DDLGQVDADA FAALEDCILN GDLSICEDVP VGNSEGDPVG  100

101  RLVNPTAAFA IDISGPAFSA TTIPPVPTLP SPELAAQLAE VYWMALARDV  150

151  PFMQYGTDDI TVTAAANLAG MEGFPNLDAV SIGSDGTVDP LSQLFRATFV  200

201  GVETGPFISQ LLVNSFTIDS ITVEPKQETF APDVNYMVDF DEWLNIQNGG  250

251  PPAGPELLDD ELRFVRNARD LARVTFTDNI NTEAYRGALI LLGLDAFNRA  300

301  GVNGPFIDID RQAGFVNFGI SHYFRLIGAA ELAQRSSWYQ KWQVHRFARP  350
                                                #       #
351  EALGGTLHLT IKGELNADFD LSLLENAELL KRVAAINAAQ NPNNEVTYLL  400

401  PQAIQEGSPT HPSYPSGHAT QNGAFATVLK ALIGLDRGGD CYPDPVYPDD  450
                  %    ##$
451  DGLKLIDFRG SCLTFEGEIN KLAVNVAFGR QMLGIHYRFD GIQGLLLGET  500
                                  #       *
501  ITVRTLHQEL MTFAEESTFE FRLFTGEVIK LFQDGTFTID GFKCPGLVYT  550

551  GVENCV
```

Figure 1. The V-BPO sequence (Swiss Prot P81701) with final numbering based on DNA sequencing, protein sequencing and electron density interpretation. Amino acid types based only on electron density interpretation are doubley underlined. Residues with special functions are in bold letters and marked with an asterisk (*), connected to vanadium atom; #, hydrogen-bonded to vanadate oxygen atoms; $, catalytic active histidine (conserved in V-CPO); and %, unique in V-BPO. Cysteine residues involved in inter-subunit disulphide bridges are in italics, all other cysteine residues are involved in intra-subunit disulphide bridges.

the water molecules $B_{\mathrm{aveWat}} = 21.7$ Å^2. The RMS deviation from the ideal bond length and angles (Engh & Huber, 1991) are 1.6° and 0.014 Å, respectively.

Two amino acid residues show unfavourable Φ/Ψ torsion angles: both Ile280, positioned in the four-residue loop between α-helices αI and αJ, have torsion angle pairs $\Phi = 67.3°$, $\Psi = -71.8°$ (IleA280) and $\Phi = 66.2°$, $\Psi = -72.2°$ (IleB280). The electron density clearly is compatible only with this conformation (Figure 3). The strained conformation, which is stabilized by a backbone hydrogen bond to Asn279, may be related to close hydrophobic side-chain contacts of Ile280 to Ile320 and Phe324. The second residue with high energy torsions angles ($\Phi = 77.4°$, $\Psi = -42.2°$) is AspB233. The conformation is fixed by a strong hydrogen bond (2.9 Å) of the backbone amide proton to the carboxyl group of AspB149, which in turn is stabilized by a second hydrogen bond (2.9 Å) to ArgB269 N$^{\varepsilon}$.

Overall structure

The native homodimeric enzyme V-BPO is a compact ellipsoid with approximate dimensions of 90 Å × 77 Å × 75 Å. The structure of the V-BPO monomer is dominated by helical secondary structure elements, as shown in Figure 4. The secondary structure assignment, based on PROCHECK (Laskowski *et al.*, 1993), is presented in Table 1. The monomer chain contains 18 α-helices and eight short β-strands with the first four β-strands arranged in two anti-parallel β-sheets and the second four β-strands in one anti-parallel β-sheet,

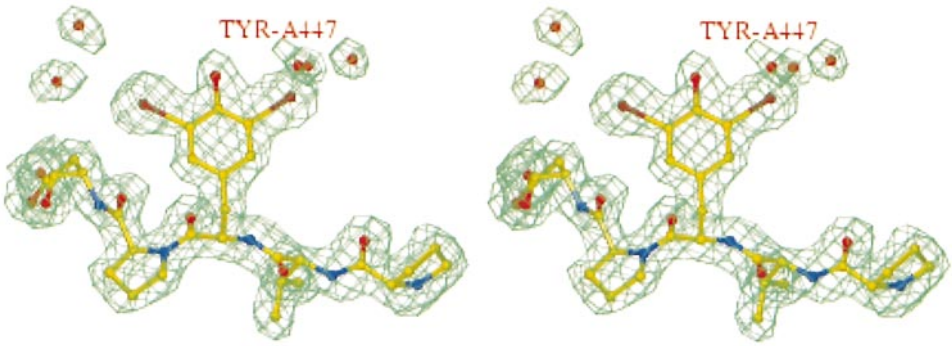

Figure 2. Final SigmaA weighted $2mF_o - DF_c$ electron density of iodinated tyrosine TyrA447. Both iodine atoms were refined with an occupancy of 0.5. The Figure was prepared with O (Jones *et al.*, 1991).

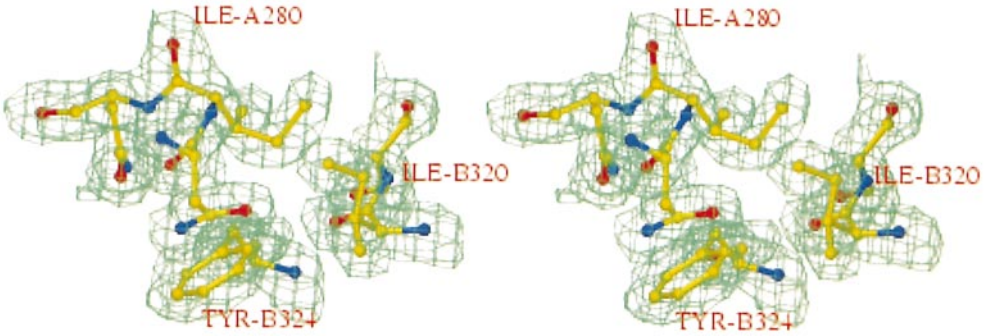

Figure 3. Final SigmaA weighted $2mF_o - DF_c$ electron density of IleA280. The Figure was prepared with O (Jones *et al.*, 1991).

located at the C-terminal end. Each monomer has three intra-molecular disulphide bridges (Cys77/Cys86, Cys441/Cys462, Cys544/Cys555) and the two molecules of the dimer are covalently linked by two additional inter-molecular disulphide bridges (CysA3/CysB41, CysA41/CysB3).

The core of the dimer consists of two four-helix-bundles (α-helices αJ, αK, αO and αQ of each monomer) (Figures 4 and 5), and six additional long helices (α-helices αA, αI and αR of each monomer). Residues of helices αK and αO of both four-helix bundles interact with each other in the dimer interface. This causes deviations from the ideal four-helix bundle packing, especially in the case of helix αK, which has a 3_{10}-helical turn in the middle at residues Ala330 to Ala333. Helices αA are aligned anti-parallel with each other at the top of the dimer (Figures 4 and 5) and connect the two V-BPO monomers at their ends with the two inter-molecular disulphide bridges. The longest, 25 residues containing α-helix αR, flanks the two four-helix bundles on the back side opposite the dimer interface. While these helices (α-helix αA, αI, αJ, αK, αO, αQ and αR) form the compact, rigid core of the structure (Figures 4 and 5), the rest of the helices (α-helix αB, αC, αD, αE, αF, αG, αH, αL, αM, αN and αP) form a less compact and less regular cap on both sides of the dimer. The active site is part of the core structure with vanadium bound as vanadate at the N-terminal end of α-helix αO.

Dimer interface

The comparison of the solvent-accessible dimer surface calculated by GRASP (Nicholls *et al.*, 1993) of 35,406 Å^2 with the monomer surfaces of 22,992 Å^2 (monomer A) and 23,078 Å^2 (monomer B) gives a calculated contact area of 10,664 Å^2. The involvement of more than 46 % of each monomer surface in the dimer interface is a structural reason for the observed high temperature (de Boer *et al.*, 1987) and chemical stability (Vilter *et al.*, 1983; Vilter, 1983b; Wever *et al.*, 1985) of the V-BPO enzyme. In addition to the two disulphide bridges

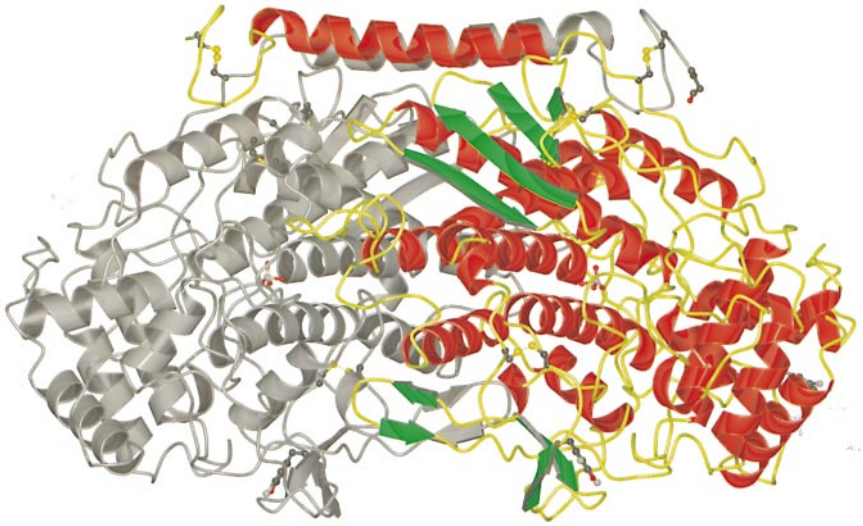

Figure 4. Ribbon-type representation of the V-BPO dimer. Monomer A, α-helices in red, β-strands in green and coil in yellow. Monomer B in gray; cystine, vanadate, pyro-glutamate and iodinated tyrosine in ball-and-stick. The Figure was drawn with MOLSCRIPT (Kraulis, 1991) and rendered with gl_render (L. Esser, unpublished: esser@ch-op.swmed.edu) and POV-Ray™.

Table 1. Secondary structure assignments

Secondary structure element	Amino acids	Secondary structure element	Amino acids
α-Helix αA	Pro15-Thr37	α-Helix αL	Pro350-Lys262
α-Helix αB	Asp67-Asn80	α-Helix αM	Leu371-Leu374
α-Helix αC	Leu83-Glu87	α-Helix αN	Ala377-Gln390
α-Helix αD	Pro132-Ala147	**α-Helix αO**	**Gly417-Ile433**
α-Helix αE	Asp159-Gly170	α-Helix αP	Leu435-Gly438
α-Helix αF	Pro190-Gln193	β-Strand β_3	Pro445-Asp449
α-Helix αG	Gln210-Val213	β-Strand β_4	Lys454-Phe458
β-Strand β_1	Phe216-Ile218	**α-Helix αQ**	**Phe465-Leu483**
β-Strand β_2	Ile221-Val223	α-Helix αR	Arg488-Thr512
α-Helix αH	Phe240-Gln247	β-Strand β_5	Ser517-Arg522
α-Helix αI	Ala268-Thr277	β-Strand β_6	Glu527-Gln533
α-Helix αJ	**Thr282-Gly293**	β-Strand β_7	Thr536-Asp540
α-Helix αK	**Ile320-Trp342**	β-Strand β_8	Phe542-Cys544

α-Helices of four-helix bundles are in boldface.

in the N-terminal region, the monomers are linked by four well-defined salt-bridges, 22 side-chain/side-chain and 66 side-chain/main-chain or main-chain/main-chain hydrogen bonds. The very stable compact structure of the V-BPO homo-dimer may be the reason for the discrepancies between earlier results of molecular mass determinations by ultra-centrifugation, SDS-PAGE under denaturing conditions and by analytical gel chromatography, which lead to an underestimated molecular mass of 95-106 kDa for the homo-dimer (Tromp *et al.*, 1990; Krenn *et al.*, 1989; Vilter, 1983b; de Boer *et al.*, 1986). Also, the molecular mass for the V-BPO monomer was estimated by several SDS-PAGE experiments in a broad range of 40-70 kDa (Wever *et al.*, 1985; Krenn *et al.*, 1989), although we have to mention that differences in the preparation of the enzyme samples for SDS-PAGE exist.

Vanadate binding site: the active centre

The vanadate is bound at the end of a 15 Å deep substrate funnel, on the N-terminal side of α-helix αO, which belongs to the four-helix bundle. The central vanadium atom is coordinated trigonal-bipyramidally (Figure 6) by its four oxygen atoms and the axially binding $N^{\varepsilon 2}$ of His486, which is stabilized by hydrogen bonds at His486 $N^{\delta 1}$ to Asp490 $O^{\delta 2}$ (2.8 Å) and to Ser413 O (2.9 Å). The nitrogen-vanadium bond length, which was not restrained in the refinement, is 2.11 Å in both monomers. The refined covalent bond distances between the four oxygen ligands and the vanadium atom are listed in Table 2. A stereo-view of the active centre and the corresponding SigmaA weighted $2mF_o - DF_c$ electron density map is given in Figure 6, demonstrating the good quality

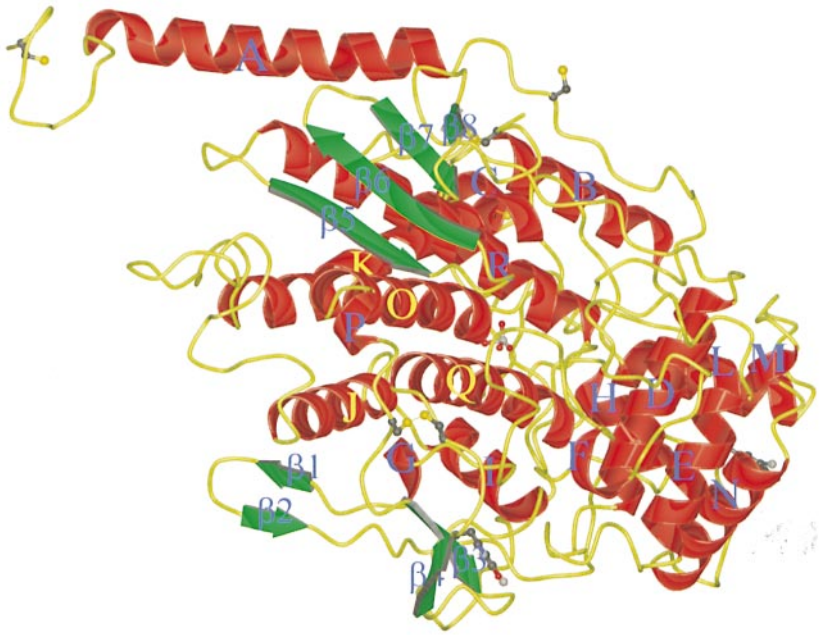

Figure 5. Ribbon-type representation of a V-BPO monomer with secondary structure assignments. α-Helices in red, β-strands in green and coil in yellow; cystine, vanadate and iodinated tyrosine in ball-and-sticks. α-Helices of the four-helix bundle are named with yellow letters. The Figure was drawn with MOLSCRIPT (Kraulis, 1991) and rendered with gl_render (see Figure 4) and POV-Ray™.

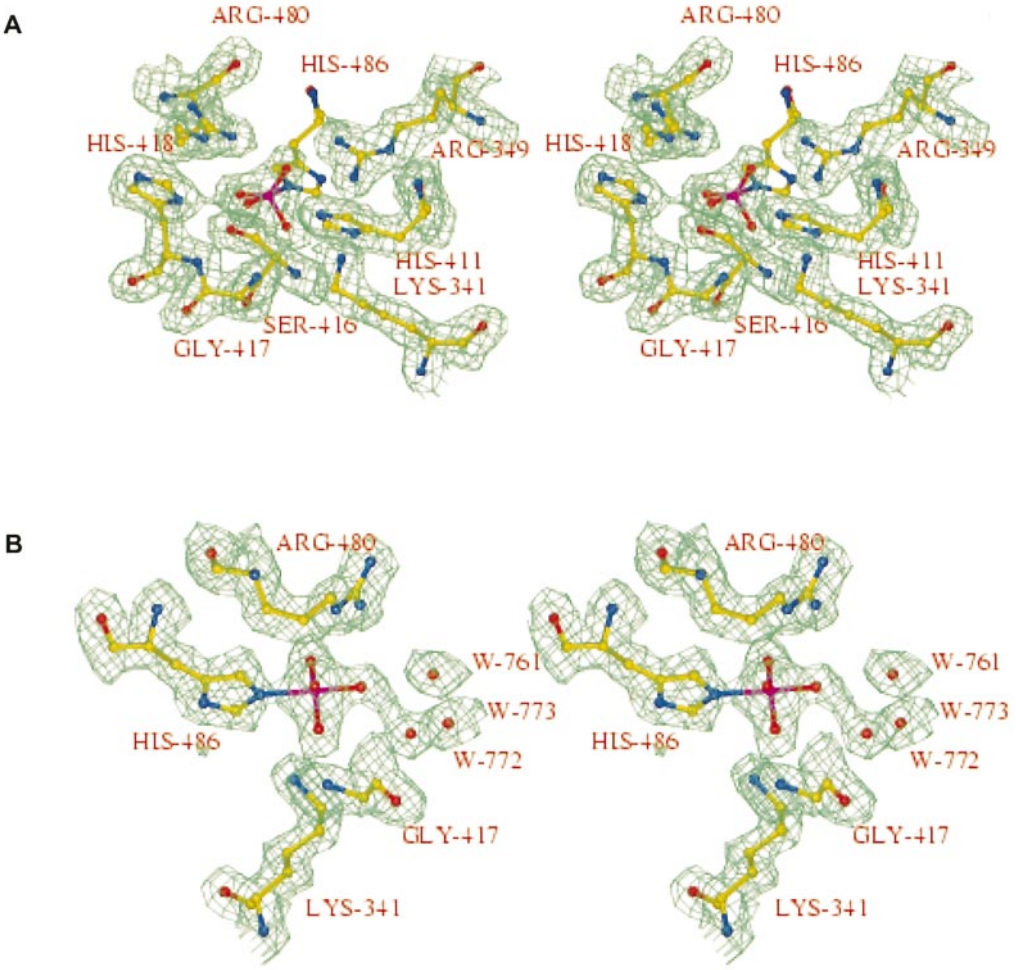

Figure 6. Final SigmaA weighted $2mF_o - DF_c$ electron density of the vanadate-binding centre. (a) View from the solvent funnel onto the active centre and (b) side-view. The Figure was prepared with O (Jones *et al.*, 1991).

of the map and the clear definition of the prosthetic group. The negatively charged vanadate group is bound *via* several hydrogen bonds (Table 3) with six nitrogen atoms and one oxygen atom of the protein acting as proton donors (Figure 7). The central part of the vanadate-binding site is formed by the first three residues of helix αO (Gly416 N, Ser417 O^{γ} and His418 $N^{\varepsilon 2}$) with additional contacts *via* Lys341 N^{ζ}, Arg349 $N^{\eta 1}$ and $N^{\eta 2}$, and Arg480 $N^{\eta 2}$.

The substrate funnel of each active centre is formed by amino acid residues from both monomers. The funnel has a diameter of ~12 Å at the entrance and ~8 Å near the axial vanadate O^4, allowing easy access of substrate molecules to the active centre. Both hydrophilic and hydrophobic residues are involved in the funnel surface, with hydrophobic residues dominating the lower part of the funnel near the vanadate-binding site.

Table 2. Bond distance at the vanadium atoms

Bond type	Monomer A (Å)	Monomer B (Å)
V-O^1	1.59	1.54
V-O^2	1.60	1.59
V-O^3	1.52	1.57
V-O^4	1.77	1.77
V-$N^{\varepsilon 2}$ His468	2.11	2.11

Table 3. Bonding network of the vanadate VO_4 for both V-BPO monomers

Bond between atom of amino acid and atoms of VO_4	Monomer A (Å)	Monomer B (Å)
Lys341 N^{ζ}-O^2	2.87	2.87
Arg349 $N^{\eta 1}$-O^1	2.93	2.93
Arg349 $N^{\eta 2}$-O^1	3.08	3.17
Ser416 O^{γ}-O^3	2.86	2.67
Gly417 N-O^2	2.88	2.69
His418 $N^{\delta 1}$-O^4 [a]	3.11	3.07
Arg480 N^{ε}-O^3	3.11	3.26
Arg480 $N^{\eta 2}$-O^1	3.13	3.21
Arg480 $N^{\eta 2}$-O^4	3.14	3.28
His486 $N^{\varepsilon 2}$-V	2.38	2.32
His411 $C^{\varepsilon 1}$-O^1 [b]	3.82	3.88
His411 $C^{\varepsilon 1}$-O^2 [b]	3.31	3.46
His411 $C^{\varepsilon 1}$-O^4 [b]	3.95	3.96

[a] Distance for the proposed catalytic, in V-HPOs, conserved histidine residue.

[b] Distance for the potential additional $N^{\varepsilon 2}$ H-donor; see the text.

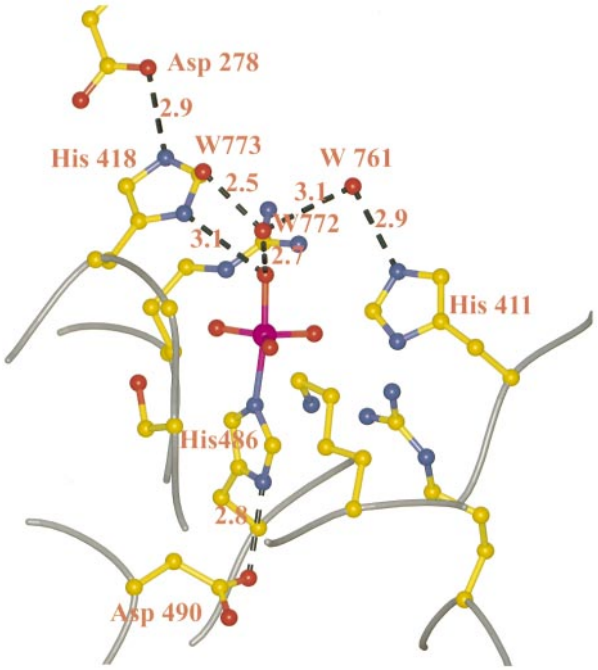

Figure 7. Hydrogen-bonding network around the vanadate centre. The Figure was drawn with MOLSCRIPT (Kraulis, 1991) and rendered with gl_render (see Figure 4) and POV-Ray™.

Within a sphere of 7.5 Å around the axial vanadate O[4], only three hydrophilic residues can be found on the funnel surface: Ser337, Gln334 and Gln421. They form hydrogen bonds among each other, but are not involved in direct interaction with the vanadate group or with hydrogen bonds to residues that bind the vanadate group. Together with the carbonyl oxygen atoms of Thr275, Asp278 and Ile280, these side-chains represent the only hydrophilic properties on the funnel surface near the vanadate group and would be available, in principle, for binding of organic compounds, which is otherwise supported only by the hydrophobic environment near the active site. However, a particular binding site near the vanadate group is presently not discernible either for small carbon compounds, like mono-chlordimedone, which is often used as a test substrate in enzymatic assays of vanadium-dependent haloperoxidases (Vilter, 1983a; de Boer *et al.*, 1988; Soedjak *et al.*, 1991), or for halide ions, like the chloride-binding tryptophan residues in haloalkane dehalogenases (Verschueren *et al.*, 1993) or α-amylases (Machius *et al.*, 1995). In addition, soaking native V-BPO crystals (see Materials and Methods) with millimolar concentrations of the substrate molecules KI and H_2O_2 produced no evidence in the electron density for specific binding of these substrates at or near the vanadate group.

The main part of the funnel surface is built of core domain amino acid residues from several regions of the V-BPO sequence. The only exceptions are Asp97, Pro98, Val99 and Val103 from the loop between helices αC and αD, which participate in the outer part of the substrate funnel surface. Six residues from the loop between four-helix bundle helices αJ and αK of monomer B are involved in the funnel surface of monomer A and *vice versa*. In the outer region these are Asn298, Arg299, Ala300, Gly301 and Ile320, and in the more interior region Phe315. The dominating part of the funnel surface is built by residues of α-helix αI and the preceding loop. This includes Thr275, Phe276, Thr277 and Asn279 in the outer part, and Asp278 and Ile280 in the inner part. Also, residues Ala403, Glu405, Glu406, Ser408 and Pro409 of the loop between helices αN and αO, and Ile485 of the loop between helices αQ and αR participate in the funnel surface.

Structure comparison of V-BPO and V-CPO: a common binding site for vanadate

The structure of the vanadium-dependent chloroperoxidase from *C. inaequalis* (V-CPO) was solved by Messerschmidt & Wever (1996) as an inactive VO_3-N_3 enzyme complex (V-CPO-N_3; PDB accession code 1VNC) and the vanadate-holoenzyme (V-CPO-VO_4) and an enzyme VO_2-peroxo complex (V-CPO-O_2) have been published (Messerschmidt *et al.*, 1997). Macedo-Ribeiro, *et al.*, (1999) have reported the X-ray structures of several active-site mutants of V-CPO. Sequence alignments of V-BPO and V-CPO show only very low sequence similarity, although both structures are classified as all-helical proteins and share the four-helix bundle motif. Manual alignment of a C-terminal V-BPO sequence fragment (Vilter, 1995) and the V-CPO sequence (Messerschmidt & Wever, 1996) showed sequence identity near the vanadate-binding site of the V-CPO. However, a tertiary structure comparison of V-CPO-N_3 with the V-BPO monomer by an automatic C^α-structure fitting procedure (Lessel & Schomburg, 1994) aligns only 172 C^α-pairs out of the possible 556 C^α-pairs (Figure 8) with an RMS deviation of 1.032 Å. The active centres of both haloperoxidases show very high structural similarity in this comparison, while the overall sequence similarity of the structurally aligned amino acid residues is quite low (21.5% sequence identity, including the six residues involved in vanadate binding). However, all residues directly involved in vanadate binding are conserved (Figure 9) and both enzymes show the same vanadate-binding sequence motif P[S/A]YP**SGH**AT† on the N-terminal side of one of the four-helix bundle helices together with direct coordination of the vanadium atom to the $N^{\varepsilon 2}$ of a histidine residue ($His486^{V\text{-}BPO}$, $His496^{V\text{-}CPO}$). Nevertheless, Macedo-Ribeiro *et al.* (1999) found a tetrahedral vanadate group at the active site in a $H496A^{V\text{-}CPO}$ mutant,

† Bold letters indicate amino acid residues that are involved in vanadate binding.

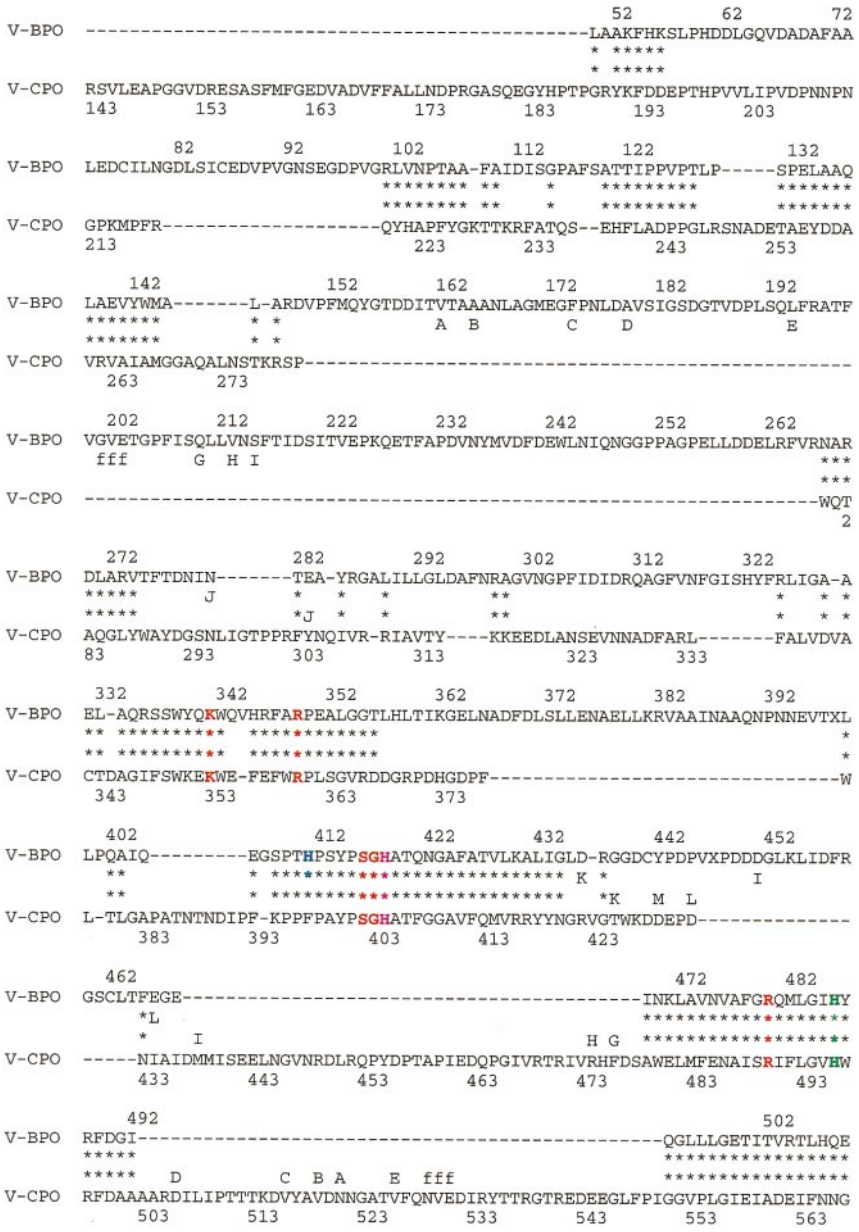

Figure 8. Structure alignment of V-CPO and V-BPO. Residues with special functions are in coloured bold letters: green, connected to vanadium atom; red, hydrogen-bonded to vanadate oxygen atoms; catalytic active histidine residues, pink (conserved in V-HPO) and blue (unique in V-BPO). C^{α}-pairs used in matrix and RMS deviation calculations are marked by asterisks (*). The tertiary structure alignment (Lessel & Schomburg, 1994) and the Figure was prepared using BRAGI (Schomburg & Reichelt, 1988).

indicating that the covalent histidine coordination is a prerequisite for the modification of the vanadium coordination with an elongated (and may be weakened) bond to the axial oxygen atom. This hypothesis agrees with the missing haloperoxidase activity of the $H496A^{V\text{-}CPO}$ mutant (Macedo-Ribeiro *et al.*, 1999). For the proposed catalytic histidine residue ($His418^{V\text{-}BPO}$, $His404^{V\text{-}CPO}$; see Figure 9) (Messerschmidt & Wever, 1996; Messerschmidt *et al.*, 1997) the RMS deviation for atoms of the imidazole ring and the C^{β} atoms is 0.02 Å in the automatic structure alignment of both enzymes, demonstrating the highly conserved vanadate binding. In the V-BPO structure, $His418^{V\text{-}BPO}$ forms a strong hydrogen bond (2.9 Å) at $N^{\eta 2}$ to the carboxyl $O^{\delta 1}$ of $Asp278^{V\text{-}BPO}$, while in V-CPO the catalytic histidine residue $His404^{V\text{-}CPO}$ is hydrogen bonded to the carbonyl oxygen atoms of $Trp289^{V\text{-}CPO}$ and $Ala290^{V\text{-}CPO}$. This different stabilization of the catalytically active histidine residue may be one structural explanation for the observed differences in halide substrate specificity (Soedjak & Butler, 1990; van Schijndel *et al.*, 1993) and pH dependencies (de Boer & Wever, 1988; van Schijndel *et al.*, 1994) of both haloperoxidases due to different p*K* values of the catalytic histidine residues.

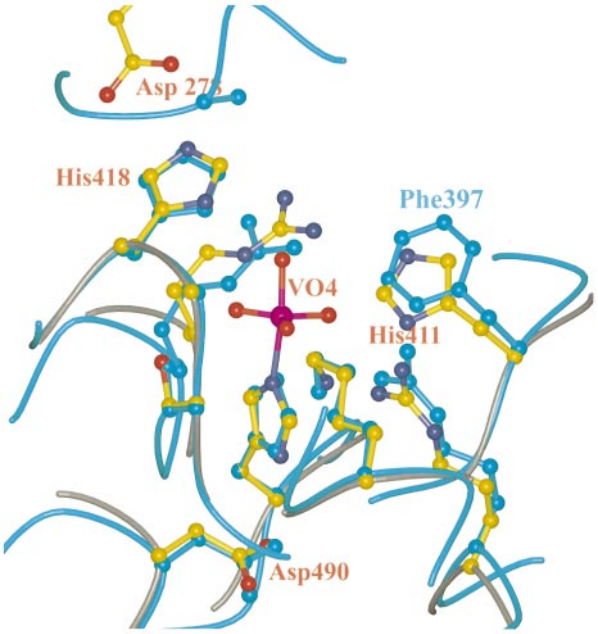

Figure 9. Superposition of V-BPO and V-CPO structures near the V-BPO vanadate group based on the secondary structure alignment of both enzymes. V-BPO residues in atom colours, V-CPO in cyan. The Figure was drawn with MOLSCRIPT (Kraulis, 1991) and rendered with gl_render (see Figure 4) and POV-Ray™.

One of the conserved arginine residues participating in vanadate binding ($R480^{V\text{-}BPO}$, $R490^{V\text{-}CPO}$) is fixed in V-BPO only by hydrogen bonds to the carbonyl oxygen atom of $Thr275^{V\text{-}BPO}$ and two water molecules, whereas it appears to be more strongly fixed in V-CPO by a salt-bridge to $Asp292^{V\text{-}CPO}$. Surprisingly, the $D292A^{V\text{-}CPO}$ mutant shows a large decrease in chlorinating activity in comparison to the recombinant native holoenzyme (Macedo-Ribeiro *et al.*, 1999). Although the $D292A^{V\text{-}CPO}$ mutation destroys the salt-bridge to $Arg490^{V\text{-}CPO}$, the arginine side-chain adopts the same conformation but hydrogen-bonded to two new water molecules (Macedo-Ribeiro *et al.*, 1999). It remains unclear why the $D292A^{V\text{-}CPO}$ mutant shows only 2% chloroperoxidase activity after introducing a (possible) greater flexibility at $Arg490^{V\text{-}CPO}$, which is comparable to the structural conditions in V-BPO.

The second and more buried conserved arginine residue ($R349^{V\text{-}BPO}$, $R360^{V\text{-}CPO}$) as well as the third basic residue, $Lys341^{V\text{-}BPO}$ and $Lys353^{V\text{-}CPO}$, is stabilized in both V-HPO structures similarly by hydrogen bonds to carbonyl oxygen atoms.

The main difference between V-BPO and V-CPO near the vanadium-binding site occurs at $His411^{V\text{-}BPO}$, which aligns with $Phe397^{V\text{-}CPO}$ in V-CPO (Figure 9). In the V-BPO structure, $His411^{V\text{-}BPO}$ shows no direct interaction with the vanadate oxygen atoms, but forms a hydrogen bond at $N^{\varepsilon 2}$ to a water molecule (2.9 Å) located near the vanadate group, indicating that the correct conformation for the imidazole ring of $His411^{V\text{-}BPO}$ was chosen (see Table 3 and Figure 7). In this orientation, $C^{\varepsilon 1}$ has a contact distance of approximately 3.4 Å from the vanadate O^2, while $N^{\delta 1}$ lacks a hydrogen-bonding partner. In the enzyme peroxide complex V-CPO-O_2 (Messerschmidt *et al.*, 1997), the peroxide moiety is bound in a side-on fashion, directed to $Phe397^{V\text{-}CPO}$, and forms a hydrogen bond to the conserved vanadate-binding $Lys353^{V\text{-}CPO}$ (in V-BPO, $Lys349^{V\text{-}BPO}$). When modelled into the active site of V-BPO this peroxovanadate group would be within hydrogen-bonding distance of $His411^{V\text{-}BPO}$ $N^{\delta 1}$ and this residue therefore may act as an additional proton donor/acceptor for the VO_2-peroxo species.

Interestingly, the structural superposition aligns α-helices of monomer A, whose atom coordinates were used in the calculation of the superposition matrix, to α-helices of V-CPO, and aligns the four-helix bundle and the α-helix αR of monomer B to corresponding V-CPO α-helices. The four four-helix bundle helices of the second V-BPO monomer thus have counterparts in one of helices of the second four-helix bundle in V-CPO. In spite of the low sequence similarity between both enzymes, this conserved structure motif and the conserved vanadium-binding features emphasize the close relationship between both vanadium-dependent haloperoxidases and may be evidence for a common genetic origin

Structure comparison of V-BPO and V-CPO: a common reaction mechanism for halide oxidation?

The X-ray structures of several forms of vanadium-dependent haloperoxidases, including two native holo-enzymes, an inhibited azide complex and a peroxo-substrate complex allow the discussion of a common mechanism for the oxidation of halide ions to hypohalides (Figure 10), which is the primary reaction catalysed by this enzyme class (van Schijndel *et al.*, 1994; Vilter, 1995). In both holoenzyme structures, V-BPO and V-CPO-VO_4 (Messerschmidt *et al.*, 1997), the axial oxygen atom is singly bound to the vanadium atom (V-BPO bond distance 1.77 Å compared to the average bond distances for the equatorial oxygen atoms of 1.57 Å; see Table 3) and forms a hydrogen bond to the conserved residues $His411^{V\text{-}BPO}$ and $His404^{V\text{-}CPO}$. This is in agreement with steady-state kinetic investigations (de Boer & Eever, 1988; van Schijndel *et al.*, 1994), which showed for both enzymes at physiological pH the reaction of hydrogen peroxide with an unprotonated enzyme species (Figure 10(a)). In the first step of the catalytic reaction mechanism proposed by Messerschmidt *et al.* (1997) this weakly bound hydroxyl group is replaced by other molecules (Figure 10(b)) either in a two-step process by release into solvent after protonation and subsequent coordination to its emptied site or in a con-

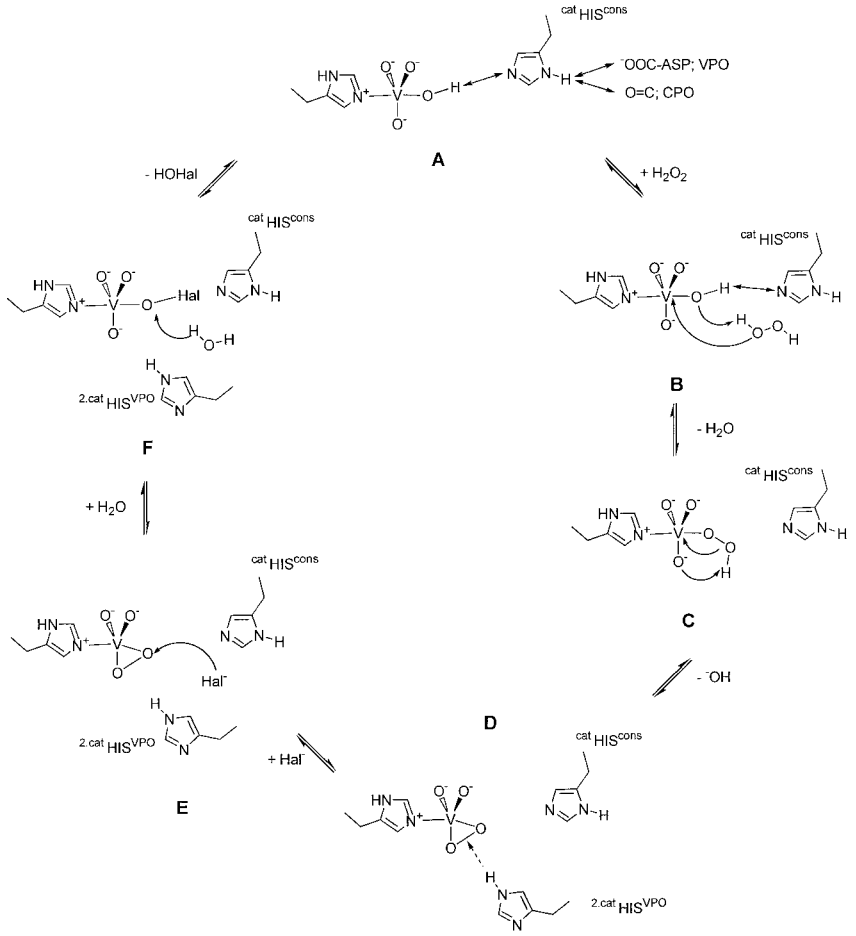

Figure 10. Proposal of a common reaction mechanism for the halide oxidation by vanadium-dependent haloperoxidases. See Discussion.

certed way by direct attack at the vanadium atom. Anyway, the possibility of replacing the axial oxygen atom is demonstrated by the stable V-CPO-VO_3-N_3 complex, achieved by Messerschmidt & Wever (1996) by soaking V-CPO apoenzyme crystals in Na_3VO_4 solution using sodium azide-containing buffers, and most likely the initial step in formation of the vanadium-peroxo complex by hydrogen peroxide is similar.

The formation of a vanadium-peroxo complex in the first reaction step is found also by steady-state kinetics at pH 6 and pH 7 for both haloperoxidases (de Boer & Wever, 1988; van Schijndel *et al.*, 1994). The V-CPO-O_2 structure shows the peroxo group bound side-on (Messerschmidt *et al.*, 1997), consistent with the more than 35 structures of small vanadium-(V)-peroxo complexes found in the Cambridge Structure Database (Allen & Kennard, 1993). Therefore, one of the original vanadate oxygen atoms has to leave the vanadium coordination sphere as a hydroxyl ion or as water, probably abstracting the second hydrogen peroxide proton (Figure 10(c)). The second peroxide oxygen atom has to be coordinated simultaneously to the vanadium centre, leading to the observed side-on peroxo species. This vanadium-peroxo complex is now able to oxidize the halide ions (Figure 10(d)). The direct coordination of halide ions to the vanadium atom suggested in the proposed reaction mechanism for V-CPO (Messerschmidt *et al.*, 1997), would be in disagreement with the results of ^{51}V and ^{127}I-NMR studies on V-BPO (Vilter *et al.*, 1990; Rehder *et al.*, 1991), which indicate no direct binding to the vanadium atom, at least in the case of iodide. In addition, soaking experiments with both V-BPO substrates, potassium iodide and hydrogen peroxide, provided no indication for an iodinated vanadium species. For these reasons, and assuming a similar reaction mechanism for both vanadium-dependent haloperoxidases in accordance with the highly conserved vanadate binding motif, we suggest a halide ion coordination to the peroxo ligand instead of a direct vanadium coordination (Figure 10(e)). The attack of the halide ion on one of the peroxide oxygen atoms would lead to the cleavage of the oxygen-oxygen peroxide bond and to the formation of an axial vanadium-OHal complex (Figure 10(f)), which is corroborated by spectrophotometric studies for both enzymes (de Boer & Wever, 1988; van Schijndel *et al.*, 1994).

The chloroperoxidase activity of V-BPO has been shown to be significantly lower than the activity of V-CPO (Vilter, 1995). This biochemical difference between V-BPO and V-CPO in the oxidation of halide ions (Soedjak & Butler, 1990; van Schijndel *et al.*, 1993; Vilter, 1995) can be attributed to the

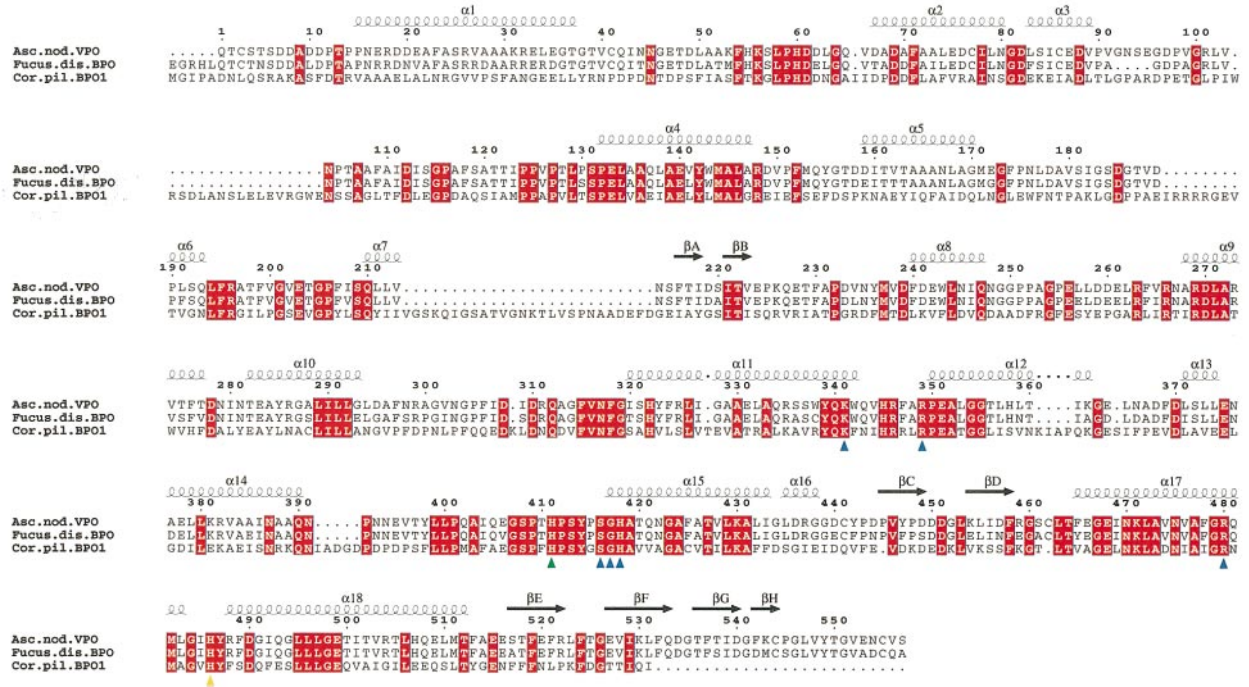

Figure 11. Sequence alignment of V-BPO class haloperoxidases. Asc.nod.V-BPO, haloperoxidase from *Ascophyllum nodosum*; Fucus_dis.BPO, bromoperoxidase from *Fucus distichus*, overall sequence similarity 89.2 % and identity 86.6 % (Vreeland *et al.*, 1998); Cor.pil.BPO1, bromoperoxidase from *Corallina pilulferia*, overall sequence similarity 42.5 % and identity 32.9 % (Shimonishi *et al.*, 1998). Conserved residues in all three sequences are in white capitals on a red background, residues that occur in at least two sequences are in red capitals, surrounded by light-blue boxes. Top lines, secondary structure and residue numbering of the present V-BPO structure. Bottom line, residues classified in accordance with the V-BPO structure: Coloured triangles; blue, vanadate H-bonding residues; orange, covalent link of the VO4 vanadate group; green, unique histidine residue of the V-BPO class peroxidases. The Figure was drawn with ESPript (P. Gouet, E. Courcelle, D. Stuart & F. Metoz. Unpublished program to analyse multiple sequence alignments in Postscript; e-mail manu@ipbs.fr; ftp server: ftp.ipbs.fr/ESPrit).

second histidine residue, $His411^{V\text{-}BPO}$, which is in close contact to the peroxo-vanadate complex (Figures 9 and 10(d)-(f)). In contrast to V-CPO (and in accordance with our proposed reaction mechanism), this histidine residue can protonate in V-BPO the bound peroxide in the vanadium-peroxo complex and may cleave the peroxide, leading to an inactive VO3-OH species, or could at least alter the redox potential of the peroxo complex in such a way that the oxidation of chloride ions is no longer efficient.

For V-BPO and the bromoperoxidase from *Corallina pilulifera*, the halogenation of organic indole compounds without intermediate formation of hypohalides (Tschirret-Guth & Butler, 1994) and the enantioselective sulphoxidation of aromatic substituted sulphide derivates (ten Brink *et al.*, 1998) has been reported in addition to the oxidation of halides. With the V-CPO enzyme, in contrast, the sulphoxidation is not enantioselective (ten Brink *et al.*, 1998). The reason for these different reactions is still unclear but may be the consequence of reasonably specific binding of these substrates on the hydrophobic surface near the vanadate-binding centre and/or of the different reactivity due to the second histidine residue, $His411^{V\text{-}BPO}$, in the active centre.

Sequences of vanadium-dependent haloperoxidases

Several other vanadium-dependent haloperoxidase sequences of eukaryotic organisms have been found and a sequence alignment with the GCG software (Version 9.0) (Genetic Computer Group, 1996) indicates two distinct sequence classes, each including the sequence of one of the presently known V-HPO structures. The V-CPO sequence, on one side, shares high sequence similarities of 97.5 % and 70.2 % to the sequence from the fungus *Embellisia didymospora* (Barnett *et al.*, 1998) and to the sequence fragment from the fungus *Drechslera biseptata* (Hemrika *et al.*, 1997) (alignment not shown). The sequence of V-BPO, on the other side, shares sequence similarities of 40.9 % and 42.5 % to sequences of two bromoperoxidases from *C. pilulifera* (Shimonishi *et al.*, 1998) and the high sequence similarity of 89.2 % to the sequence of a bromoperoxidase from *Fucus distichus* (Vreeland *et al.*, 1998). The sequence alignment for this class of V-BPOs is shown in Figure 11, indicating the conserved vanadate-binding residues, which are found also in sequences of the V-CPO structure class. Interestingly, all enzymes of the V-BPO class are classified as bromoperoxidases and show the additional

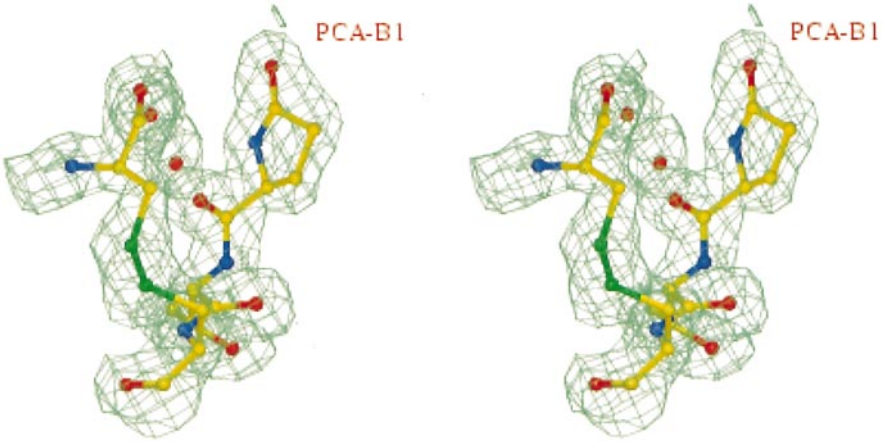

Figure 12. The N terminus of V-BPO monomer B: model of the pyroglutamate in the final SigmaA weighted $2mF_o - DF_c$ electron density. The Figure was prepared with O (Jones *et al.*, 1991).

second histidine residue near the active site, indicating the importance of this residue for substrate specificity (Figure 11). Furthermore the quite high sequence similarity within both sequence classes is good evidence for high structural similarity to one of the known V-BPO structures. In the case of the bromoperoxidase from *F. distichus* even all cysteine residues, which are involved in disulphide bridges in the V-BPO structure, are conserved (Figure 12) and the structure of this bromoperoxidase therefore should be highly similar to the V-BPO structure.

The vanadate-binding sequence motif, generalized to **K**X_6**R**P$X_{10\text{-}52}$ (A/S/G) (Y/F) P**SGH** (T/A) $X_{30\text{-}53}$ (S/G) **R**X_5 **H** (W/Y/F/H) XXDX_3G, has been found also in bacterial acid phosphatases (Hemrika *et al.*, 1997; Neuwald, 1997), mammalian glucose-6-phosphatases and several lipid phosphatases (Stukey & Carman, 1997). For V-CPO, very low phosphatase-activity has been reported (Hemrika *et al.*, 1997) and for V-BPO it is known that treatment of apoenzyme with phosphate buffers inhibits the haloperoxidase activity (Vilter, 1995). This sequence motif seems to be a common binding motif for threefold negatively charged tetrahedral ions adapted for at least two different activities.

Materials and Methods

DNA sequencing

Algal material, isolation of poly(A)$^+$ mRNA and construction of a cDNA library

Ascophyllum nodosum was collected on the Atlantic coast (Roscoff, France). Poly(A)$^+$ RNA were purified from total RNA by hybridization of the 3′ poly(A) region of the mRNA to a biotinylated oligo(dT) primer and capture of the hybrid with streptavidin coupled to paramagnetic particles, according to the Promega protocol (Poly ATtract mRNA Isolation System). cDNA was synthesized using a cDNA synthesis kit (Pharmacia, standard protocol) and cloned into the *Eco*RI site of the lambda vector NM1149 (Murray, 1983). The resulting phage DNA was packaged *in vitro* into phages particles using Gigapack II packaging extract from Stratagene.

Isolation and sequencing of cDNA clones

The cDNA library from *A. nodosum* was screened with end-labelled, eightfold degenerate 14-mer and 64-fold degenerate 17-mer oligodesoxynucleotides encoding the amino acid motif FMQYG and HYRFDG, respectively. Hybridizations were performed at 27 °C overnight in 6 × SSPE, 0.08 % (w/v) PVP, 0.08 % (v/v) Ficoll, 0.1 % (w/v) SDS and the labelled oligonucleotide. Filters were washed twice at 27 °C in the same buffer without radioactive probe. cDNA insertions obtained from the purified lambda phage were subcloned into the *Eco*RI of pBluescript-SK. The sequencing was performed by the dideoxy chain reaction termination method (Pharmacia) on double-stranded DNA using universal pSK or gene-specific primers.

Peptide sequencing: chemical and enzymatic cleavages

Chemicals

CNBr and iodoacetamide were purchased from Merck; trypsin, endoproteinase Lys-C and endoproteinase Glu-C were from Boehringer Mannheim; DTT and ammonium bicarbonate were from Sigma; trifluoroacetic acid (TFA) and urea were from Fluka. All reagents used for protein sequencing and amino acid analysis were from Applied Biosystems.

Cyanogen bromide cleavage

V-BPO (100 µg) was dissolved in 100 µl of 70 % (v/v) formic acid containing 7 mg of CNBr and incubated for 24 hours at room temperature in the dark under nitrogen (Gross & Witkop, 1961). After dilution with 1 ml of water, the sample was dried in a Speedvac. The peptide fragments were dissolved in 50 % (v/v) acetonitrile containing 0.1 % TFA and separated by reverse-phase HPLC on a Vydac C4 column (4.6 mm × 150 mm) with a gradi-

ent from 5 % to 95 % acetonitrile containing 0.1 % TFA in 45 minutes at a flow-rate of 0.8 ml/minute.

Cleavage with trypsin, endoproteinase Glu-C, and endoproteinase Lys-C

V-BPO (100 μg) was dissolved in 50 ml of 8 M urea, 0.4 M ammonium bicarbonate and reduced with 5 μl of 45 mM DTT at 50 °C for 15 minutes (Stone & Williams, 1993). Cysteine residues were alkylated by the addition of 5 μl of 100 mM iodoacetamide and incubation at room temperature in the dark for 15 minutes. After dilution with 140 μl of water, 2 μg of trypsin and 5 μg of endoproteinase Glu-C or 1 μg of endoproteinase Lys-C were added and incubated for 24 hours at 37 °C (trypsin and Lys-C) or room temperature (Glu-C). Peptides were separated on a Vydac C18 column (4.6 mm × 150 mm) or an Aquapore OD-300 C18 column (1.0 mm × 100 mm).

Sequence analysis

Peptides were collected in microcentrifuge vials, dried in a Speedvac, redissolved in 50 % acetonitrile and applied to Biobrene-treated, precycled glass-fibre filters and sequenced by automated Edman degradation with Applied Biosystems 470A and 494A Procise (gas-phase) or 473A (pulsed-liquid) sequencers with on-line HPLC detection of PTH amino acids.

Mass spectrometry

Mass spectra of peptides were measured on a Finnigan TSQ700 triple stage quadrupole mass spectrometer equipped with an electrospray source. For LC/MS, an Applied Biosystems 172A microbore HPLC with an Aquapore OD-300 C18 column (1.0 mm × 100 mm) was operated at a flow-rate of 40 μl/minute with a gradient of acetonitrile containing 0.06 % TFA in water. The m/z range from 350 to 2000 was continuously scanned in three seconds.

Amino acid analysis

The amino acid composition of V-BPO and peptide fragments was analyzed on an Applied Biosystems 420A/H analyser by automated gas-phase hydrolysis with 6 M HCl at 160 °C for 75 minutes and precolumn derivatization with PITC.

Crystallization and crystallographic data collection

V-BPO was purified from native cell-material in a large-scale process, consisting of a three-step liquid-liquid extraction, dialysis and hydrophobic interaction and anion-exchange chromatography Vilter (1994). Apoenzyme was prepared by dialysis of holoenzyme according to Vilter 1984. Crystals of the holoenzyme and the apoenzyme were obtained from 2.1 M ammonium sulfate solutions buffered at pH 8.3 and diffracted to 2.4 Å (1 Å = 0.1 nm) resolution (Weyand *et al.*, 1996). The crystals were stable in the X-ray beam for more than one week. They belong to the tetragonal system, space group $P4_32_12$, with lattice constants $a = 114.3$ Å, $c = 276.0$ Å. The choice of the space group was later confirmed by visual inspection of the first interpretable electron density map, which showed the correct hand for several well-defined α-helices. The asymmetric unit contains one homo-dimer of 556 residues and one vanadate group per monomer with a solvent content, calculated according to Matthews (1968), of 67 % (v/v).

The structure solution was performed by isomorphic replacement using tungstate as heavy-atom derivative. It was assumed that the tungstate moiety binds at the same site as the vanadate moiety in the holoenzyme, which was proved by Messerschmidt & Wever (1998) in the case of V-CPO and we found an equivalent result for V-BPO. Data sets of holoenzyme (*NATIVE I*), apoenzyme (*APO*) and a tungsten derivative (*WO4 I*) were collected using a Xentronics area detector and graphite monochromated CuK_α radiation of a Siemens rotating anode operated at 45 kV and 100 mA (Table 4). All data sets were collected on a Siemens four-axis goniometer with a crystal-to-detector distance of 280 mm and a 0.3 mm collimator. Crystals were mounted with the *c*-axis parallel with the oscillation axis. The data sets were measured at three settings, two high-resolution ($2\Theta = 22°$) settings and one low-resolution setting ($\Theta = 12°$) at constant Φ angle. High-resolution settings were separated by a 30° rotation in the χ angle. The data for each setting are composed of 300 frames with a frame width of ten minutes arc. The exposure time for a frame was 12 minutes (15 minutes for the tungsten derivative) for high-resolution data and ten minutes for low-resolution data. All measurements were carried out at 283 K. The frames were processed using the XENGEN program system (Howard, 1990) and scaled in batches of 4° rotation using the CCP4 program system (CCP4, 1994).

An additional high-resolution native dataset (*Native III*) was collected at 130 K (Table 4). Crystals of the native holoenzyme were soaked for 24 hours in cryo buffer containing 25 % (v/v) glycerol, 2.2 M $(NH_2)_2SO_4$, 50 mM Tris-HCl (pH 7.8) and the two substrates, 10 mM H_2O_2 and 10 mM KI. Crystals were mounted on a cryo-loop and shock-frozen in a stream of evaporating liquid nitrogen. The X-ray intensities were processed with CERIUS/XGEN (Biosym/MSI, 1996) and programs from the CCP4 program suite (CCP4, 1994). Crystal parameters and data collection statistics are given in Table 5.

Further data sets of the holoenzyme (*Native II*) and the tungsten derivative (*WO4 II*) were collected at the beamline BW6 of the DESY synchrotron using monochromatized radiation at $\lambda = 1.0$ Å, a κ-goniometer and an MAR imaging plate detector (Table 5). The crystal-to-detector distance was 430 mm for the native and 370 mm for the derivative data collection. The scan angle was 1.0° for all measurements. The data were processed with DENZO (Otwinowski & Minor, 1996) and scaled with SCALEPACK (Otwinowski & Minor, 1996). Because of strong spot overlapping, only reflections to 2.9 Å were used. Table 4 gives a summary of data collection, processing, and scaling statistics of the finally used data sets.

Heavy-atom refinement and phasing

The structure factor amplitudes of the tungsten derivative were scaled to the native data by the program FHSCAL (CCP4, 1994). The positional parameters of the tungsten-binding site were obtained from a difference Patterson map calculated with FFT (CCP4, 1994). This map was analysed by the program RSPS (CCP4, 1994). Heavy-atom sites were refined by the vector-space refinement program VECREF (CCP4, 1994) and phase sets were calculated by the program MLPHARE (CCP4, 1994).

Table 4. Haloperoxidase V-BPO X-ray data set statistics; rotating anode measurements, λ = 1.54 Å

	Native I	Apo	WO4 I
$T_{meas.}$ (K)	283	283	283
Soaking conditions	-	-	15 mM Na_2WO_4; 2 days
Space group	$P4_32_12$	$P4_32_12$	$P4_32_12$
Unit cell constants (Å)	$a = 114.3$, $c = 276.0$	2a = 114.3, $c = 276.0$	$a = 114.3$, $c = 276.0$
Max. resolution (Å)	2.8	2.95	2.8
$I/\sigma(I)$	10.7/(5.7)[a]	8.3/(5.1)[a]	8.2/(6.1)[a]
R_{merge} (%)	5	6.8	6.5
R_{iso} (%) (Native 1)		8.3	-
R_{PH} (%) (Apo)			12.1
	Number of observed reflections/percentage of unique reflections/redundancy		
Overall	**39232/85.9/1.9**	**32518/81.2/2.4**	**30096/65.3/4.7**
Last shell	3069/47.6/1.4	2744/45.1/2.4	2837/43.4/2.4

	Native III
$T_{meas.}$ (K)	130
Soaking conditions	10 mM KI, 10 mM H_2O_2; 12 hours
Space group	$P4_32_12$
Unit cell constants (Å)	a=113.2, c=272.3
$I/\sigma(I)$	9.4/(5.2)[a]
R_{merge} (%)	6.1
	Number of obs. refl./percentage of unique refl./redundancy
Overall	**105642/95.0/2.3**
Last shell	13696/85.7/1.4

$$R_{\text{merge}} = \frac{\sum_h \sum_i |I(h)_i - \langle I(h)\rangle|}{\sum_h \sum_i I(h)_i}$$

$$R_{\text{PH}} = \frac{\sum_h |F(h)_{\text{deriv}} - F(h)_{\text{nat}}|}{\sum_h F(h)_{\text{nat}}}$$

(15.0 Å to 3.0 Å).
[a] In last resolution shell.

Scaling and phasing of the rotating anode derivative data (*WO4 I*) against apoenzyme (*APO*) and the synchrotron derivative data set (*WO4 II*) against holoenzyme (*Native II*) in the resolution range 3.0 to 15.0 Å was done separately (Table 6). Combination of the two phase sets with SIGMAA (CCP4, 1994) increased the figure of merit from 0.23 and 0.29 to 0.31.

Table 5. Haloperoxidase V-BPO data set statistics; synchrotron measurements, λ = 1.0 Å

Data set	*Native II*	*WO4 II*
Soaking conditions	-	15 mM Na_2WO_4; 2 days
Space group	$P4_32_12$	$P4_32_12$
Unit cell constants (Å)	$a = 113.2$, $c = 272.3$	$a = 113.2$, $c = 272.3$
$T_{meas.}$ (K)	283	277
Max. resolution (Å)	2.9	2.9
R_{merge} (%)	6.4	9
R_{PH} (%)	-	14.1
Number of observed reflections/percentage of unique reflections		
Overall	**35,906/87.2**	**36,129/88.3**
Last shell	1791/31.0	4851/83.6

Density modifications and determination of non-crystallographic symmetry (NCS)

An early attempt to determine the NCS axis by self-rotation searches showed at a level of 2.5σ only the crystallographic symmetry axes and several unconvincing results at a level of 1.5σ. Therefore the combined phase set was used in a first density modification run with DM (CCP4, 1994) to calculate a molecular envelope of the V-BPO dimer using the solvent-flattening and histogram-mapping option, and under the assumption of a solvent content of approximately 65 %. This dimer solvent mask was analysed using the graphic program O (Jones *et al.*, 1991). In this mask, the boundaries of the homodimer were clearly visible and the 2-fold NCS axis could be identified. The position of the NCS axis was refined manually by real-space averaging with IMP from the RAVE program package (Jones, 1992). This final orientation corresponded to one of the peaks in a self-rotation map contoured at the 1σ level.

Phase improvement of the combined SIR-phases was then repeated including NCS-averaging. This improved the figure of merit for reflections in the resolution range from 15.0 Å to 3.0 Å from 0.31 for the combined phase set to 0.81. The resulting electron density map, calculated with this improved phases and the structure factor amplitudes of native data set *Native I*, showed clearly identifiable helices that confirmed the choice of the correct enantiomorphic space group $P4_32_12$.

Table 6. Haloperoxidase V-BPO derivative refinement statistics

Derivative	Native data set	$^1R_{cullis}$ (%) acentr./centr.	Atom	x	y	z	Binding site
$NaWO_4$; WO_4 1	*APO*	82/69	W 1	0.832	0.367	0.093	Active site monomer A
			W 2	0.568	0.223	0.033	Active site monomer B
$NaWO_4$; WO_4 2	*Native II*	89/80	W 1	0.832	0.367	0.093	Active site monomer A
			W 2	0.568	0.223	0.033	Active site monomer B

		Figure of merit	Number of reflections (15-3.0 Å)
Phase calculation (15-3.0 Å)	*APO*	0.2865	24,341
	Native II	0.2328	31,853
	Combined on *Native I*	0.3118	34,626

$$R_{\text{Cullis}} = \frac{\sum_h |F_{\text{PHcalc}}(h) - F_{\text{PHobs}}(h)|}{\sum_h |F_{\text{PHobs}}(h)|}$$

Electron density map interpretation

Combined phases weighted by the figure of merit (f.o.m.) were used to calculate an electron density map for 10.0 to 3.0 Å data. Interpretation of this map, using the graphics program O (Jones *et al.*, 1991), was based on skeletonized electron density calculated by the program BONES (Jones, 1992). The starting *R*-value for this initial model consisting of 519 contiguous residues, taken as alanine due to the initial lack of a known sequence, was 51.6 % in the resolution shell 10.0 to 3.0 Å. The initial refinement, using the program XPLOR (Brünger, 1992), reduced the *R*-value to 42.0 %.

A refinement cycle in this phase consisted of an energy-refinement step, simulated annealing according to the slow-cooling protocol, followed by another energy-refinement step. The refined coordinates were then used to refine the NCS operator using the RAVE package (Jones, 1992).

At this stage, the quality of the electron density allowed the unambiguous identification of sequence fragments obtained by DNA or peptide sequencing. Iteration of this procedure of cyclic model building, positional refinement and refinement of the NCS operator allowed the identification of 554 residues and the VO_4 group. Equilibrium bond distances and bond angles for the vanadate group were taken from hydrogen vanadate (Aschwanden *et al.*, 1993). Inclusion of all known sequence fragments yielded a continuous amino acid sequence for Pro15 to Val556 with two inter-molecular disulphide bridges and three intra-molecular disulphide bridges. The *R*-value for this model was 25.1 % at 2.8 Å.

Refinement of the model

The V-BPO-refinement was continued with the high-resolution data set *Native III* and 5 % of the reflections of the high-resolution data set were separated for R_{free} calculations. After one rigid body refinement cycle, calculated with XPLOR (Brünger, 1992), the final refinement to maximum resolution of 2.05 Å was done with cyclic model building and restrained maximum likelihood refinement calculations using REFMAC (CCP4, 1994). During the final refinement cycles, no restraint was used for the vanadate group: 1787 water molecules were determined from SigmaA weighted $mF_o - DF_c$ density maps manually and using the ARP procedure (Lamzin & Wilson, 1993).

From previous protein sequencing results it was known that the V-BPO sequence was N-terminally blocked (Vilter, 1995). Inspection of the SigmaA weighted $2mF_o - DF_c$ map showed clear indication of a pyroglutamate residue at the N terminus of monomer B (Figure 11), which is fixed by crystallographic contacts, but not at the N-terminus of monomer A. The resulting complete amino acid sequence of V-BPO is shown in Figure 1, whereas in this final V-BPO model the amino acid types of the first 14 residues are based only on the observed SigmaA weighted $2mF_o - DF_c$ electron density map.

Data deposition

The final V-BPO is deposited at the SWISS-Protein sequence database under the accession code P81701 and the coordinate structure factors are deposited at the Protein Data Bank (http://www.rcsb.org) under the PDB accession code 1QI9.

Acknowledgements

We thank Katrin Opolka for expert technical assistance and Dr Bernard Kloareg (Station Biologique de Roscoff, France) for generous use of laboratory space and equipment. H.V. thanks the DFG for generous scholarship. This work was funded by DFG grants VI 91/5-1 and VI 91/5-2.

References

Allen, F. H. & Kennard, O. (1993). 3D search and research using the Cambridge structural database. *Chem. Des. Autom. News*, **8**, 31-37.

Aschwanden, S., Schmalle, H. W., Reller, A. & Oswald, H. R. (1993). Preparation, crystal structure, thermal and catalytic behaviour of copper divanadate. *Mater. Res. Bull.* **28**, 575-579.

Barnett, P., Hemrika, W., Dekker, H. L., Muijsers, A. O., Renirie, R. & Wever, R. (1998). Isolation, characterization, and primary structure of the vanadium

chloroperoxidase from the fungus *Embellisia didymospora*. *J. Biol. Chem.* **273**, 23381-23287.

Biosym/MSI, (1996). *Crystallographic Workbench X-GEN Users Guide*, , San Diego, CA.

Brindley, A. A., Dalby, A. R., Isupov, M. N. & Littlechild, J. A. (1998). Preliminary X-ray analysis of a new crystal form of the vanadium-dependent bromoperoxidase from *Corallina officinalis*. *Acta Crystallog. sect. D,* **54**, 454-457.

Brünger, A. T. (1992). *XPLOR, Version 3.1: A System for Crystallography and NMR*, Yale University Press, New Haven, CT.

CCP4, (1994). Collaborative computational project, number 4. The CCP4 suite: programs for protein crystallography. *Acta Crystallog. sect. D,* **50**, 760-763.

de Boer, E. & Wever, R. (1988). The reaction mechanism of the novel vanadium-bromoperoxidase, a steady-state kinetic analysis. *J. Biol. Chem.* **263**, 12326-12332.

de Boer, E., van Kooyk, Y., Tromp, M. G. M., Plat, H. & Wever, R. (1986). Bromoperoxidase from *Ascophyllum nodosum*: a novel class of enzymes containing vanadium as a prosthetic group?. *Biochim. Biophys. Acta,* **869**, 48-53.

de Boer, E., Plat, H., Tromp, M. G. M., Wever, R., Franssen, M. C. R., Van der Pas, H. C., Meijer, E. M. & Schoemaker, H. E. (1987). Vanadium containing bromoperoxidase - an example of an oxidoreductase with high operational stability in aqueous and organic media. *Biotech. Bioeng.* **30**, 607-610.

de Boer, E., Boon, K. & Wever, R. (1988). Electron paramagnetic resonance studies on conformational states and metal ion exchange properties of vanadium bromoperoxidase. *Biochemistry,* **27**, 1629-1635.

Engh, R. A. & Huber, R. (1991). Accurate bond and angle parameters for X-ray protein structure refinement. *Acta Crystallog. sect. A,* **47**, 392-400.

Genetic Computer Group (1996). *Wisconsin Package Version 9.0*, Madsion, WI.

Gross, E. & Witkop, B. (1961). Selective cleavage of the methionyl peptide bonds in ribonuclease with cyanogen bromide. *J. Am. Chem. Soc.* **83**, 1510-1511.

Hemrika, W., Renirie, R., Dekker, H. L., Barnett, P. & Wever, R. (1997). From phosphatases to vanadium peroxidases: a similar architecture of the active site. *Proc. Natl Acad. Sci. USA,* **94**, 2145-2149.

Howard, A. (1990). *The Xengen System*, Genex Corporation, Gaithersburg.

Jones, T. A. (1992). A, yaap, asap, @#*? A set of averaging programs. In *Molecular Replacement* (Dodson, E. J., Gover, S. & Wolf, W., eds), pp. 91-105, , Warrington, SERC Daresbury Laboratory.

Jones, T. A., Zou, J. Y., Cowan, S. W. & Kjelgaard, M. (1991). Improved methods for building protein in electron density maps and the location of errors in these models. *Acta Crystallog. sect. A,* **47**, 110-119.

Kraulis, P. J. (1991). MOLSCRIPT: a program to produce both detailed and schematic plots of protein structures. *J. Appl. Crystallog.* **24**, 946-950.

Krenn, B. E., Tromp, M. G. & Wever, R. (1989). The brown alga *Ascophyllum nodosum* contains two different vanadium bromoperoxidases. *J. Biol. Chem.* **264**, 19287-19292.

Küpper, F. C., Schweigert, N., Ar, Gall E., Legendre, J.-M., Vilter, V. & Kloareg, B. (1998). Iodine uptake in *Laminariales* involves extracellular, haloperoxidase-mediated oxidation of iodide. *Planta,* **207**, 163-171.

Lamzin, V. S. & Wilson, K. S. (1993). Automated refinement of protein models. *Acta Crystallog. sect. D,* **49**, 129-147.

Laskowski, R. A., MacArthur, M. W., Moss, D. S. & Thornton, J. M. (1993). PROCHECK: a program to produce both detailed and schematic plots of protein structures. *J. Appl. Crystallog.* **26**, 283.

Lessel, U. & Schomburg, D. (1994). Similarities between protein 3-D structures. *Protein Eng.* **7**, 1175-1187.

Macedo-Ribeiro, S., Hemrika, W., Renirie, R., Wever, R. & Messerschmidt, A. (1999). X-ray crystal structures of active site mutants of the vanadium-containing chloroperoxidase from the fungus *Curvularia inaequalis*. *J. Biol. Inorg. Chem.* **4**, 209-219.

Machius, M., Wiegand, G. & Huber, R. (1995). Crystal structure of calcium-depleted *Bacillus licheniformis* alpha-amylase at 2.2 Å resolution. *J. Mol. Biol.* **246**, 545-559.

Matthews, B. (1968). Solvent content of protein crystals. *J. Mol. Biol.* **33**, 491-497.

Messerschmidt, A. & Wever, R. (1996). X-ray structure of a vanadium-containing enzyme: chloroperoxidase from the fungus *Curvularia inaequalis*. *Proc. Natl Acad Sci. USA,* **93**, 392-396.

Messerschmidt, A. & Wever, R. (1998). X-ray structures of apo and tungstate derivatives of vanadium chloroperoxidases from the fungus *Curvularia inaequalis*. *Inorg. Chim. Acta,* **273**, 160-166.

Messerschmidt, A., Prade, L. & Wever, R. (1997). Implications for the catalytic mechanism of the vanadium-containing enzyme chloroperoxidase from the fungus *Curvularia inaequalis* by X-ray structures of the native and peroxide form. *Biol. Chem.* **378**, 309-315.

Müller-Fahrnow, A., Hinrichs, W., Saenger, W. & Vilter, H. (1988). The first crystallization of a vanadium-dependent peroxidase. *FEBS Letters,* **239**, 292-294.

Murray, N. E. (1983). Phage lambda and molecular cloning. In *Lambda II Monograph* (Hendrix, R. W., ed.), vol. 13, pp. 395-432, Cold Spring Harbor Laboratory Press, Cold Spring Harbor, NY.

Neuwald, A. F. (1997). An unexpected structural relationship between integral membrane phosphatases and soluble haloperoxidases. *Protein Sci.* **6**, 1764-1767.

Nicholls, A., Bharadwaj, R. & Honig, B. (1993). GRASP-graphical representation and analysis of surface properties. *Biophys. J.* **64**, A166.

Otwinowski, Z. & Minor, W. (1996). Processing of X-ray diffraction data collected in oscillation mode. In *Methods in Enzymology* (Carter, C. W. & Sweet, R. M., eds), vol. 276, pp. 307-325, Academic Press, London.

Rehder, D., Holst, H., Priebsch, W. & Vilter, H. (1991). Vanadate-dependent bromo/iodoperoxidase from *Ascophyllum nodosum* also contains unspecific low-affinity binding sites for vanadate(V): a ^{51}V-NMR investigation, including the model peptides Phe-Glu and Gly-Tyr. *J. Inorg. Biochem.* **41**, 171-185.

Rush, C., Willetts, A., Davies, G., Dauter, Z., Watson, H. & Littlechild, J. (1995). Purification, crystallisation and preliminary X-ray analysis of the vanadium-dependent haloperoxidase from *Corallina officinalis*. *FEBS Letters,* **359**, 244-246.

Schomburg, D. & Reichelt, J. (1988). BRAGI: a comprehensive protein modelling program system. *J. Mol. Graph.* **6**, 161-165.

Shimonishi, M., Kuwamoto, S., Inoue, H., Wever, R., Ohshiro, T., Izumi, Y. & Tanabe, T. (1998). Cloning

and expression of the gene for a vanadium-dependent bromoperoxidase from a marine macro-alga, *Corallina pilulifera*. *FEBS Letters,* **428**, 105-110.

Simons, B. H., Barnett, P., Vollenbroek, E. G. M., Dekker, H. L., Muijsers, A. O., Messerschmidt, A. & Wever, R. (1995). Primary structure and characterization of the vanadium chloroperoxidase from the fungus *Curvularia inaequalis*. *Eur. J. Biochem.* **229**, 566-574.

Soedjak, H. S. & Butler, A. (1990). Chlorination catalyzed by vanadium bromoperoxidase. *Inorg. Chem.* **29**, 5017-5025.

Soedjak, H. S., Everett, R. R. & Butler, A. (1991). The novel non-heme vanadium bromoperoxidase from marine algae: phosphate inactivation. *J. Industr. Microbiol.* **8**, 37-44.

Stone, K. L. & Williams, K. R. (1993). Enzymatic digestion of proteins and HPLC peptide isolation. In *A Practical Guide to Protein and Peptide Purification for Microsequencing* (Matsudaira, P., ed.), pp. 45-69, Academic Press, London.

Stukey, J. & Carman, G. M. (1997). Identification of a novel phosphatase sequence motif. *Protein Sci.* **6**, 469-472.

ten Brink, H. B., Tuynman, A., Dekker, H. L., Hemrika, W., Izumi, Y., Oshiro, T., Schoemaker, H. E. & Wever, R. (1998). Enantioselective sulfoxidation catalyzed by vanadium haloperoxidases. *Inorg. Chem.* **37**, 6780-6784.

Tromp, M. G. M., Olafsson, G., Krenn, B. E. & Wever, R. (1990). Some structural aspects of vanadium bromoperoxidase from *Ascophyllum nodosum*. *Biochim. Biophys. Acta,* **1040**, 192-198.

Tschirret-Guth, R. A. & Butler, A. (1994). Evidence for organic substrate binding to vanadium bromoperoxidase. *J. Am. Chem. Soc.* **116**, 411-412.

van Schijndel, J. W. P. M., Vollenbroeck, E. G. M. & Wever, R. (1993). The chloroperoxidase from the fungus *Curvularia inaequalis*-a novel vanadium enzyme. *Biochim. Biophys. Acta,* **1161**, 249-256.

van Schijndel, J. W. P. M., Barnett, P., Roelse, J., Vollenbroeck, E. G. M. & Wever, R. (1994). The stability and steady-state kinetics of vanadium chloroperoxidase from the fungus *Curvularia inaequalis*. *Eur. J. Biochem.* **225**, 151-157.

Verschueren, K. H. G., Franken, S. M., Rozeboom, H. J., Kalk, K. H. & Dijkstra, B. W. (1993). Refined X-ray structures of haloalkane dehalogenase at pH 6.2 and pH 8.2 and implications for the reaction mechanism. *J. Mol. Biol.* **232**, 856-872.

Vilter, H. (1983a). Peroxidases from Phaeophyceae. III. Catalysis of halogenation by peroxidases from *Ascophyllum nodosum* (L.) Le Jol. *Bot. Mar.* **26**, 429-435.

Vilter, H. (1983b). Peroxidases from Phaeophyceae. IV. Fractionation and location of peroxidases isoenzymes in *Ascophyllum nodosum* (L.) Le Jol. *Bot. Mar.* **26**, 451-455.

Vilter, H. (1984). Peroxidases from Phaeophyceae. A vanadium(V)-dependent peroxidase from *Ascophyllum nodosum*. *Phytochemistry,* **23**, 1387-1390.

Vilter, H. (1994). Aqueous two phase systems. In *Methods in Enzymology* (Walter, H. & Johannson, G., eds), vol. 282, pp. 665-672, Academic Press, London.

Vilter, H. (1995). Vanadium-dependent haloperoxidases. In *Metal Ions in Biological Systems-Vanadium and Its Role in Life* (Sigel, H. & Sigel, A., eds), vol. 31, pp. 325-353, Marcel Dekker, Inc., New York, Basel.

Vilter, H., Glombitza, K.-W. & Grawe, A. (1983). Peroxidases from Phaeophyceae. I. Extraction and detection of the peroxidases. *Bot. Mar.* **26**, 331-340.

Vilter, H., Takahashi, S., Sato, K., Wälchi, M. R. & Hosoya, T. (1990). Iodine I^{127}-NMR studies on vanadium-dependent peroxidase from the brown alga *Ascophyllum nodosum*. In *SAMBAS III, Bosen*, vol. 46, Saarland, Germany.

Vreeland, V., Ng, K. L. & Epstein, L. (1998). CDNA sequence and active recombinant vanadium bromoperoxidase from *Fucus embryos*. *Mol. Biol. Cell,* **9**, 1043.

Wever, R., Plat, H. & De Boer, E. (1985). Isolation procedure and some properties of the bromoperoxidase from the seaweed *Ascophyllum nodosum*. *Biochim. Biophys. Acta,* **830**, 181-186.

Weyand, M., Hecht, H.-J., Vilter, H. & Schomburg, D. (1996). Crystallization and preliminary X-ray analysis of a vanadium-dependent haloperoxidase from *Ascophyllum nodosum*. *Acta Crystallog. sect. D,* **52**, 864-865.

Edited by R. Huber

(Received 14 June 1999; received in revised form 6 September 1999; accepted 6 September 1999)